

# The better distant phosphor configurations for enhancing WLED color intensity: $\text{YVO}_4:\text{Eu}^{3+}$ and $\text{YF}_3:\text{Mn}^{2+}$

Ha Thanh Tung<sup>1</sup>, Huu Phuc Dang<sup>2</sup>

<sup>1</sup>Faculty of Basic Sciences, Vinh Long University of Technology Education, Vinh Long Province, Vietnam

<sup>2</sup>Faculty of Fundamental Science, Industrial University of Ho Chi Minh City, Ho Chi Minh City, Vietnam

## Article Info

### Article history:

Received Nov 29, 2021

Revised Jul 30, 2022

Accepted Dec 27, 2022

### Keywords:

Correlated color temperature

Mie-scattering theory

Phosphor structure

$\text{YF}_3:\text{Mn}^{2+}$

$\text{YVO}_4:\text{Eu}^{3+}$

## ABSTRACT

The distant phosphor configuration produces more illuminating beams than the two settings containing conformal or in-cup phosphor. When this configuration is used, though, it is difficult to manage the color standard of light-emitting diodes (LEDs). As a result, in past few years, numerous studies have focused on controlling the color standard of distant phosphor configurations. Until present, two distant phosphor configurations of single- and triple-film phosphor configurations, have been used to improve color standards. This research will investigate the ideal configuration among these configurations in terms of color rendering index (CRI), color quality scale (CQS), lumen output (LO), as well as color homogeneity for multi-chip white LEDs (WLEDs). WLEDs, operating at five different temperatures of color between 5600 K and 8500 K, are used to perform the studies. The results reveal that the three-sheet phosphor setting would be more desirable, with greater CRI, CQS, and lumen efficiency (LE) indexes. Furthermore, when using a triple-layer phosphor arrangement, color variation is reduced, resulting in a rise in color consistency. This conclusion is possibly verified by using Mie theory to analyze scattering properties in distant phosphor setup, making the study findings legitimate and important data to produce more advanced WLEDs.

This is an open access article under the [CC BY-SA](https://creativecommons.org/licenses/by-sa/4.0/) license.



## Corresponding Author:

Huu Phuc Dang

Faculty of Fundamental Science, Industrial University of Ho Chi Minh City

No. 12 Nguyen Van Bao Street, Ho Chi Minh City, Vietnam

Email: danghuuphuc@iuh.edu.vn

## 1. INTRODUCTION

Light-emitting diodes (LEDs) are considered the next-generation luminous origin and have been increasingly popular over the years due to their numerous benefits, including excellent illuminating efficiency, eco-friendliness, small design, and extended lifetime [1], [2]. White LEDs are made in one of two ways: one, by combining single-color chips of LED with multiple colors (typically blue, red, and green), and the other, by combining said chips with phosphor, especially phosphor-converted LEDs (pcLEDs) [3]. According to the excellent illumination performance of the following [4]-[6], the most auspicious pcLED configuration is one that uses a blue-pumping III-nitride-based LED chip as the excitation supply and a yellow-phosphor of  $\text{Ce}^{3+}$ -doped YAG (or YAG:Ce) as the illuminator. The phosphor configuration has a massive effect on pcLED optic efficiencies, such as illuminating efficacy (IE), angular chromatic homogeneity (ACH), and chroma rendering intent (CRI), among other things. As a result, investigators have statistically investigated the impacts of applied phosphors on pcLEDs with regard to particle size [7], doped weight percentage [8], attenuation coefficient [9], and structural morphologies [10]-[12]. The majority of the researchers use the Monte Carlo method [13] to facsimile illuminating spreading within the phosphor layer, with the Mie dispersion template [14]

solving the optic characteristics of the phosphor. Furthermore, the Mie template necessitates the accurate setting of various microscopic parameters throughout the simulation, some of which are difficult to obtain. Furthermore, though the phosphor film also contains non-spherical granules, the Mie template is a precise scattering computation for uniform globular granules [11], [15], [16]. As a result, the simulation findings for both output blue and yellow lightings, as well as their angular dispersion, might not match the experimental results, making it difficult to estimate the pcLEDs' luminous intensity correctly. Zaman *et al.* [17] as well as Kim *et al.* [18] utilized the formation containing the dual integrating sphere to analyze the radiated strength of the transferred and reflected illumination of a YAG:Ce film under a fiber-optic guided excitation or of a phosphor-film sequence to provide accurate optic simulation, and enhance the Mie parameters in optic modeling for pcLEDs, respectively. Chen *et al.* [19] created a 1-D architecture to compute luminous absorbance and transformation in the phosphor layer, which White *et al.* [20] enhanced by taking the dispersion impact into consideration. However, the emitted illumination's angular distribution was ignored in the previous studies. The computed bidirectional scattering distribution function (BSDF) was developed by Lazidou *et al.* [21], Zhou *et al.* [22] and Wei *et al.* [23] to quantify optic characteristics of the phosphor layer. For the yellow and blue light distributing intensity, the simulated findings demonstrate great accord with the experiments. Most significantly, in comparison with the Mie-theory-based bulk scattering technique, the BSDF model can accurately predict illumination distributions with no addressing luminous scattering and absorption activities within the phosphor-film sequence. This model is not restricted by the particle form of doped phosphors and may significantly reduce modeling time. Li *et al.* [24] also presented a planar illuminating setup applying BSDF statistics. Li *et al.* [24] used BSDF on a pcLED configuration to acquire an accurate emission luminous energy result, and subsequently improved the combining gap in the module [25], [26]. Nevertheless, the prior BSDF model does not account for variable phosphor concentration and thickness, which can have a significant impact on illumination scattering and absorption [27], [28], making it difficult to use in pcLEDs with a variety of phosphor configurations. The optic characteristics of YAG phosphor layers with different concentrations and thicknesses are metered in this research. On the BSDF distributions, the effects of concentration and thickness were addressed. The obtained data was utilized to create the BSDF model, which took into account the modifying values of phosphorus concentration and layer thickness within the experimental range. Eventually, the model will be used in modeling a cylindrical pcLED, ensuring its precision and efficiency.

## 2. SIMULATION DETAILS

### 2.1. Preparing essential phosphors

YF<sub>3</sub>:Mn<sup>2+</sup> particles with an emission peak of 2.38 and 2.60 eV and emission color of green are increasingly common in the phosphor conversion field. The factors that affect the YF<sub>3</sub>:Mn<sup>2+</sup> phosphors' luminescence feature include their sizes of granules as well as concentration. YVO<sub>4</sub>:Eu<sup>3+</sup> are the second particles to be mentioned. They have an emission peak of 2.00 eV which is known as a type of red phosphor. It is possible to get well-prepared YVO<sub>4</sub>:Eu<sup>3+</sup> particles by using required ingredients with precise concentrations in mole and weight, as shown in Table 1. If YVO<sub>4</sub>:Eu<sup>3+</sup> is to be created, a process consisting of three main steps of firing must be strictly followed. First, combine all the ingredients by dry grinding or milling. After that, the firing step begins by firing the materials within open quartz boats in the condition of air under the temperature of 1000 °C within 1 hour and powderize them. And this is followed by the next two firing steps. The second firing step is quite similar to the first step but at 1200 °C. The materials are powdered again, washed by NaOH (or KOH) mixed with water. The products are washed for multiple times using pure water and leave them to dry. Eventually, the final firing step takes place as the second step, also within open quartz boats in the condition of air under the temperature of 1200 °C within 1 hour.

Table 1. Ingredients of YVO<sub>4</sub>:Eu<sup>3+</sup> phosphor composition

Ingredient	Mole (%)	By weight (g)
Y <sub>2</sub> O <sub>3</sub>	95 (of Y)	107
Eu <sub>2</sub> O <sub>3</sub>	5 (of Eu)	8.8
Nh <sub>4</sub> VO <sub>3</sub>	110	129

### 2.2. Simulation process

The WLEDs with nine LED chips manufactured internally are used in this study, with 1.16 W radiating power at a 453-nm peak wavelength for each chip. The single-layer distant phosphor configuration (SL) with a yellow phosphor layer YAG:Ce<sup>3+</sup> coating the outside of LED chips is shown in Figure 1(a). Figure 1(b) shows a triple-layer distant configuration (TL) with a YF<sub>3</sub>:Mn<sup>2+</sup> phosphor layer placed between two additional phosphor layers.

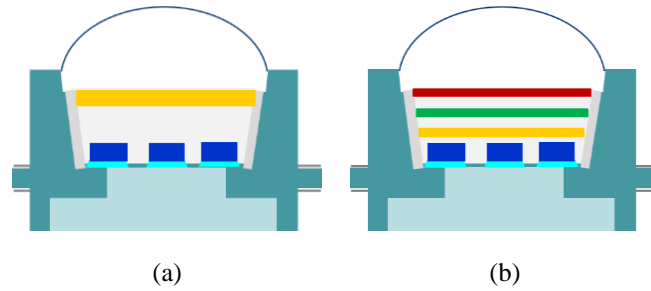


Figure 1. Multi-layer phosphor packages' simulation for WLEDs: (a) Single-layer phosphor and (b) triple-layer phosphor

All sheets of phosphor are 0.08-mm thick. If we want to sustain the correlated temperature colors (ACCTs) at an average level, the concentration of YAG:Ce must be modified when the red or green phosphor concentration varies. It's also worth noting that the YAG:Ce concentrations differ depending on which ACCT is used and which phosphor configuration is used. As a result of this, the scattering characteristics of LEDs differ, resulting in a wide range of optic features.

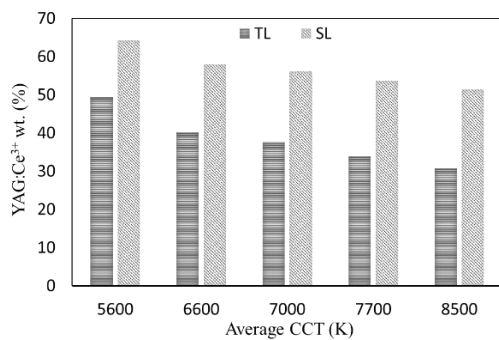


Figure 2. Concentrations of YAG:Ce phosphor in TL and SL setups for every average CCT

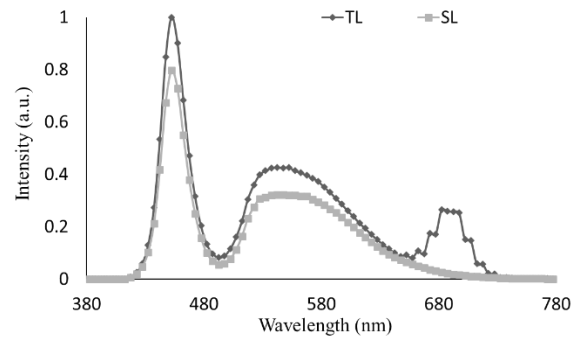


Figure 3. The intensity of emission in TL and SL setups

Figure 2 shows that the yellow YAG:Ce<sup>3+</sup> phosphor concentration performs outstanding increases at every ACCT level in the SL configuration but the greater reduced amounts in the TL configuration. When all distant phosphor configurations are examined at a given ACCT, the greater the YAG:Ce<sup>3+</sup> content probably leads to more occurring back-scattering, and the illuminating beam reduces as a consequence. On the other hand, as said content reaches a significant level, a disparity between the three major hues that create the light of white (yellow, red, and green) emerges, resulting in a loss of uniformity in color re-creation in the WLED device. For the task of acquiring superior illuminating beam as well as reproducing hue features in the WLED device, obtaining a decrease in back-scattering and maintaining the sufficiency and equal distribution of three hues of yellow, red, and green elements are significantly critical. Furthermore, raising the red spectra could support the CRI value, while the green spectra can affect color homogeneity and illuminating beam. Given the aforementioned possibilities, the triple-layer phosphor looks to be the best configuration for regulating optic features, doesn't it? the group of researchers continues to provide essential information linked to distant phosphor configurations, namely the emission spectrum, in order to address this question. As demonstrated in Figure 3, the emission spectrum of distant phosphor configurations differs noticeably. When contrasted with the other distant phosphor configurations at five distinct ACCTs, the emission spectra of the SL layout have the minimum luminosity. This proves that the SL layout is inferior to the TL in terms of illuminating beam intensity. Moreover, the TL configuration produces the best spectrum strength from 380 nm to 780 nm.

### 3. RESULTS AND DISCUSSION

It is possible to draw a comparison between the CRI of TL and SL setups using the data in Figure 4. Apparently, regardless of ACCT values, the TL configuration obtains the maximum CRI. The CRI value rises in tandem with the growth in ACCT, reaching its greatest point under a temperature of 8500 K. The finding could be critical when it comes to augmenting the CRI of WLEDs using distant phosphor configurations.

Moreover, the TL thrives at managing CRI at high ACCT (exceeding 7000 K), which might be a challenge to achieve. The TL configuration would be outstanding in terms of CRI benefits, or the mono-layer structure's (SL) CRI is relatively lower. Based on these findings, it can be stated that the TL configuration is the best choice for mass-produced WLEDs if the aim is CRI. Despite this, CRI can access only one aspect of color reproduction. An in-depth assessment of chromatic reproduction effects required more than a good CRI. In the past few years, numerous studies have focused on a new indicator termed CQS, which is a composite of CRI, viewer's taste, and chromatic coordinates. CQS has been deemed the most essential indicator in assessing color rendering intent and color reproduction efficiency, making it a significant and desirable achievement. CQS of distant phosphor configurations is contrasted in this research and displayed in Figure 5. The TL obviously displays the more excellent CQS results, which might be because of its greater CRI. The equilibrium of three fundamental colors: yellow, green, and red, demonstrates this outcome. If the color standard is better, the CQS value will be higher. In the meantime, unlike the CRI, the CQS value for the SL layout is largely different, specifically, much lower than the other. Generally, the SL benefits illuminating beam but not color standard control unless green and red-light portions are introduced. Although the SL layout has a downside in terms of color intensity, it is advantageous in terms of manufacturing because it is easier to produce and costs less than the remaining configurations.

It may be concluded from the results in Figure 4 that if color standards are the primary goal for producers, choosing the TL configuration can be considered. On the other hand, we need to be concerned with whether the illuminating beam becomes impacted if the color intensity is improved. To address this issue, the research group is contrasting the illuminating beam created by single-layer and dual-layer configurations. This part will give the present an explanation based on the math solution for transferred blue illumination as well as transformed yellow illumination for an SL and a dual-sheet (DL) (for the simplification of the mathematic system). This model also shows that a DL configuration can result in a significant increase in LED luminosity, meaning using more distant phosphor sheets can help increase the white-light emission intensity of the pcLED.

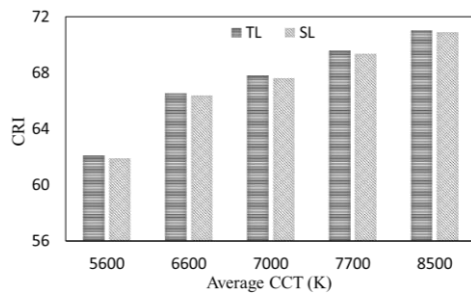


Figure 4. Color rendering indexes in TL and SL setups for every average CCT

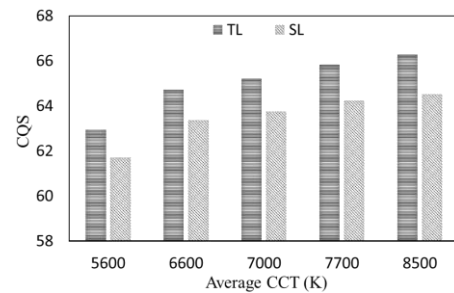


Figure 5. Color quality scale in TL and SL setups for every average CCT

The following expressions are used to compute the transferred blue illumination as well as transformed yellow illumination for the SL setup having a phosphor sheet breadth measured at  $2h$  in (1) and (2) and in the DL setup with a phosphor sheet breadth measured at  $h$  in (3) and (4).

$$PB_1 = PB_0 \times e^{-2\alpha_{B1}h} \quad (1)$$

$$PY_1 = \frac{1}{2} \frac{\beta_1 \times PB_0}{\alpha_{B1} - \alpha_{Y1}} (e^{-2\alpha_{Y1}h} - e^{-2\alpha_{B1}h}) \quad (2)$$

$$PB_2 = PB_0 \times e^{-2\alpha_{B2}h} \quad (3)$$

$$PY_2 = \frac{1}{2} \frac{\beta_2 \times PB_0}{\alpha_{B2} - \alpha_{Y2}} (e^{-2\alpha_{Y2}h} - e^{-2\alpha_{B2}h}) \quad (4)$$

Where  $h$  denotes the thickness for every phosphor sheet in the distant phosphor setups; the subscripts "1" and "2" denote SL and DL setups, respectively. When blue illumination is transmuted into yellow illumination,  $\beta$  represents the transformation coefficient.  $\gamma$  is the yellow-illumination reflection coefficient. The optical power generated by the LED in blue will be represented via the blue illumination ( $PB$ ) as well as yellow illumination ( $PY$ ) intensities, both of which will be indicated via  $PB_0$ . The optical energy loss in the lighting propagation within the setups are indicted by  $\alpha B$  for blue illumination as well as  $\alpha Y$  for yellow illumination.

The illumination effectiveness for a pcLED is clearly higher with a DL configuration than with a SL configuration:

$$\frac{(PB_2+PY_2)-(PB_1+PY_1)}{PB_1+PY_1} > 0 \quad (5)$$

At the same time, Mie dispersion hypothesis [29] is employed for the task of calculating the dispersion coefficients and cross section of spherical phosphor granules in phosphor films. Then, we can employ the law of Lambert-Beer [30] for the task of determining the transferred illumination energy.

$$I = I_0 \exp(-\mu_{ext}L) \quad (6)$$

For (6),  $I_0$  and  $I$  represent the incident illumination (strength and the transferred illumination energy, respectively).  $L$  exhibits the breadth for a phosphor sheet in millimeters).  $\mu_{ext}$  indicates the attenuation coefficient. The expression for calculating attenuation coefficient is:  $\mu_{ext} = N_r \times C_{ext}$ , with  $N_r$  ( $\text{mm}^{-3}$ ) and  $C_{ext}$  ( $\text{mm}^2$ ) correspondingly determine the density allocation number and the extinction cross-section for phosphor spheres. The (5) shows that a system with many phosphor layers improves illuminating beam more than a single layer configuration. This finding is further supported by Figure 5, which shows that the SL configuration has the least illuminating beam of the four configurations at all ACCTs. On the contrary, the TL configuration possesses the biggest light ray. Though it obtains the best producing color display, the outcome dispels any questions regarding the beneficial degree of TL configuration. As the  $\text{YAG:Ce}^{3+}$  concentration decreases, the TL configuration minimizes the quantity of backscattered illuminations. Furthermore, blue LED chip lights may effortlessly bypass the  $\text{YAG:Ce}^{3+}$  sheet, going towards the remaining sheets. As such, the TL configuration efficiently converts the blue illumination output generated by chips in LED. As a consequence, the TL configuration has the maximum spectrum strength in the white light wavelength region, resulting in the most illuminance.

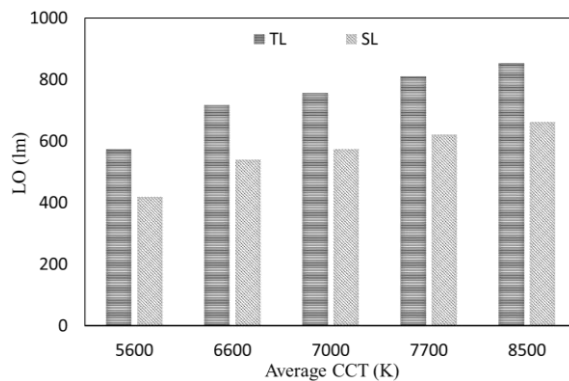


Figure 6. Lumen output (LO) in TL and SL setups for every average CCT

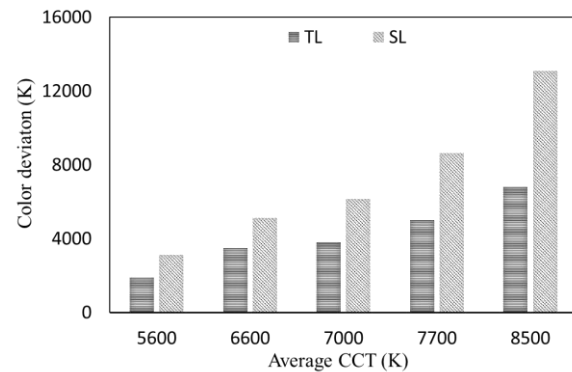


Figure 7. CCT deviation (D-CCT) in TL and SL setups for every average CCT

Because of the excellent optic characteristics of WLEDs, such as CQS and LE value, the TL configuration can be adopted. It should be noted that color homogeneity cannot be overlooked when color standard is the objective. Color homogeneity can be improved in a variety of ways, including the use of enhanced scattering particles and conformal phosphor design. Although chromatic constancy is improved, the illuminating beam may be reduced as a result of these two procedures. Using the green  $\text{YF}_3:\text{Mn}^{2+}$  phosphor and the red  $\text{YVO}_4:\text{Eu}^{3+}$  phosphor improves the white illuminating intensity by increasing the scattering characteristics and the additional green or red elements within the WLEDs, see Figure 6. Furthermore, the utilization of distant phosphor configurations improves illuminating performance by minimizing light reflection to the surface of LED chips. However, in order to produce the best transferred energy, the phosphor layer concentration should be regulated to an optimum level. The Lambert-Beer law in (6) proves this. The color divergence of distant phosphor configurations is compared in Figure 7. If the color consistency is stronger, the color divergence will be reduced. The color divergence value of the TL configuration is the lowest, as seen in the figure. This outcome can be proven by the scattering event that occurs within the LED packet before the light of white is formed. The more phosphor layers there are, the more dispersion occurs, which improves color consistency. However, increased scattering events can result in a reduction in luminance. This decrease,

however, comparing to the benefits gained by minimizing backscattering, can be seen as a small sacrifice. The reduction in backscattering is vital to both color reproduction efficiency and the function of the conversion phosphors. Accordingly, the TL configuration may achieve the greatest color consistency while maintaining the greatest light intensity. Besides that, for all ACCTs, the SL layout has the biggest color variation, indicating the large difference in color display of its white light.

#### 4. CONCLUSION

Finally, for five distinct ACCTs, this paper examines the optic effectiveness of two remote-layer phosphor configurations: SL and TL. Additionally, the modeling procedure utilizes green  $\text{YF}_3:\text{Mn}^{2+}$  phosphor and red  $\text{YVO}_4:\text{Eu}^{3+}$  phosphor. The Mie hypothesis as well as the law of Lambert-Beer are also used for the task of verifying the outcomes of the investigation. Based on these findings, complementing green LEDs with the green phosphor layer  $\text{YF}_3:\text{Mn}^{2+}$  improves color consistency and output luminosity. It's clear that the color re-generation efficiency is determined by the proportions of three fundamental colors including blue, green, red, and yellow. It is possible for the TL configuration to uniformly regulate these primary colors on the chroma scale. Furthermore, the decrease of backscattering in TL enables a significant rise in its illuminating beam. The largest value of light intensity comes from the TL configuration, which supports this conclusion. Producers can simply choose the most appropriate configuration that matches their needs relying on the findings of this study for the task of augmenting the efficiency for their WLED products.




#### REFERENCES

- [1] Y. Wu, *et al.*, "Monolithic integration of  $\text{MoS}_2$ -based visible detectors and GaN-based UV detectors," *Photonics Research*, vol. 7, no. 10, pp. 1127-1133, 2019, doi: 10.1364/PRJ.7.001127.
- [2] C. Jaques, E. Pignat, S. Calinon, and M. Liebling, "Temporal super-resolution microscopy using a hue-encoded shutter," *Biomedical Optics Express*, vol. 10, no. 9, pp. 4727-4741, 2019, doi: 10.1364/BOE.10.004727.
- [3] H. Yang, *et al.*, "Giant quantum dots encapsulated inside a freeform lens," *Applied Optics*, vol. 57, no. 35, pp. 10317-10322, 2018, doi: 10.1364/AO.57.010317.
- [4] S. Jost, C. Cauwerts, and P. Avouac, "CIE 2017 color fidelity index Rf: a better index to predict perceived color difference?," *Journal of the Optical Society of America A*, vol. 35, no. 4, pp. B202-B213, 2018, doi: 10.1364/JOSAA.35.00B202.
- [5] B. Xu, Q. Wu, Y. Bao, G. Chen, Y. Wang, and S. Ren, "Time-multiplexed stereoscopic display with a quantum dot-polymer scanning backlight," *Applied Optics*, vol. 58, no. 16, pp. 4526-4532, 2019, doi: 10.1364/AO.58.004526.
- [6] B. Jain *et al.*, "High performance electron blocking layer-free InGaN/GaN nanowire white-light-emitting diodes," *Optics Express*, vol. 28, no. 1, pp. 665-675, 2020, doi: 10.1364/OE.28.000665.
- [7] C. Su, X. Liu, and J. Zhang, "Analysis of the errors of the integrating sphere for the transmittance of nonplanar optical components," *Journal of Optical Technology*, vol. 85, no. 1, pp. 42-47, 2018, doi: 10.1364/JOT.85.000042.
- [8] M. Vanoli, M. Grassi, F. Lovati, S. Barzaghi, T. MP Cattaneo, and A. Rizzolo, "Influence of innovative coatings on salami ripening assessed by near infrared spectroscopy and aquaphotomics," *Journal of Near Infrared Spectroscopy*, vol. 27, no. 1, pp. 54-64, 2019, doi: 10.1177/0967033518811796.
- [9] F. Guan, G. Jiang, Y. Song, M. Yu, Z. Peng, F. Chen, "No-reference high-dynamic-range image quality assessment based on tensor decomposition and manifold learning," *Applied Optics*, vol. 57, no. 4, pp. 839-848, 2018, doi: 10.1364/AO.57.000839.
- [10] P. J. Pardo, M. I. Suero, and A. L. Pérez, "Correlation between perception of color, shadows, and surface textures and the realism of a scene in virtual reality," *Journal of the Optical Society of America A*, vol. 35, no. 4, 2018, doi: 10.1364/JOSAA.35.00B130.
- [11] L. Xu, B. Zhao, and M. R. Luo, "Color gamut mapping between small and large color gamuts: part II. gamut extension," *Optics Express*, vol. 26, no. 13, pp. 17335-17349, 2018, doi: 10.1364/OE.26.017335.
- [12] C. Han *et al.*, "Effect of surface recombination in high performance white-light  $\text{CH}_3\text{NH}_3\text{PbI}_3$  single crystal photodetectors," *Optics Express*, vol. 26, no. 20, pp. 26307-26316, 2018, doi: 10.1364/OE.26.026307.
- [13] Q. Song, *et al.*, "Vicarious calibration of COCTS-HY1C at visible and near-infrared bands for ocean color application," *Optics Express*, vol. 27, no. 20, pp. A1615-A1626, 2019, doi: 10.1364/OE.27.0A1615.
- [14] S. Feng and J. Wu, "Color lensless in-line holographic microscope with sunlight illumination for weakly-scattered amplitude objects," *OSA Continuum*, vol. 2, no. 1, pp. 9-16, 2019, doi: 10.1364/OSAC.2.000009.
- [15] P. P. Li, *et al.*, "Unveiling of control on the polarization of supercontinuum spectra based on ultrafast birefringence induced by filamentation," *Journal of the Optical Society of America B*, vol. 35, no. 11, pp. 2916-2922, 2018, doi: 10.1364/JOSAB.35.002916.
- [16] K. Werfli, *et al.*, "Experimental Demonstration of High-Speed  $4 \times 4$  Imaging Multi-CAP MIMO Visible Light Communications," *Journal of Lightwave Technology*, vol. 36, no. 10, pp. 1944-1951, 2018, doi: 10.1109/JLT.2018.2796503.
- [17] Q. Zaman, *et al.*, "Two-color surface plasmon resonance nanosizer for gold nanoparticles," *Optics Express*, vol. 27, no. 3, pp. 3200-3216, 2019, doi: 10.1364/OE.27.003200.
- [18] W. J. Kim *et al.*, "Improved angular color uniformity and hydrothermal reliability of phosphor-converted white light-emitting diodes by using phosphor sedimentation," *Optics Express*, vol. 26, no. 22, pp. 28634-28640, 2018, doi: 10.1364/OE.26.028634.
- [19] J. Chen, *et al.*, "Fabrication of,  $\text{Tb,Gd}_3\text{Al}_5\text{O}_{12}:\text{Ce}^{3+}$  phosphor ceramics for warm white light-emitting diodes application," *Optical Materials Express*, vol. 9, no. 8, pp. 3333-3341, 2019, doi: 10.1364/OME.9.003333.
- [20] T. P. White, E. Deleporte, and T. -C. Sum, "Feature issue introduction: halide perovskites for optoelectronics," *Optics Express*, vol. 26, no. 2, pp. A153-A156, 2018, doi: 10.1364/OE.26.00A153.
- [21] D. Lazidou, D. Lampakis, I. Karapanagiotis, and C. Panayiotou, "Investigation of the Cross-Section Stratifications of Icons Using Micro-Raman and Micro-Fourier Transform Infrared FT-IR Spectroscopy," *Applied Spectroscopy*, vol. 72, no. 8, pp. 1258-1271, 2018, doi: 10.1177/0003702818777772.
- [22] Y. Zhou *et al.*, "Comparison of nonlinear equalizers for high-speed visible light communication utilizing silicon substrate phosphorescent white LED," *Optics Express*, vol. 28, no. 2, pp. 2302-2316, 2020, doi: 10.1364/OE.383775.
- [23] T. Wei, W. Bo, C. Yan, C. Yeqing, L. Jun, and Z. Qingguang, "Single  $\text{Pr}^{3+}$ -activated high-color-stability fluoride white-light phosphor for white-light-emitting diodes," *Optical Materials Express*, vol. 9, no. 1, pp. 223-233, 2019, doi: 10.1364/OME.9.000223.




- [24] P. P. Li, *et al.*, “Very high external quantum efficiency and wall-plug efficiency 527 nm InGaN green LEDs by MOCVD,” *Optics Express*, vol. 26, no. 25, pp. 33108-33115, 2018, doi: 10.1364/OE.26.033108.
- [25] T. Han, *et al.*, “Spectral broadening of a single Ce<sup>3+</sup>-doped garnet by chemical unit cosubstitution for near ultraviolet LED,” *Optical Materials Express*, vol. 8, no. 12, pp. 3761-3769, 2018, doi: 10.1364/OME.8.003761.
- [26] X. Liu, *et al.*, “Laser-based white-light source for high-speed underwater wireless optical communication and high-efficiency underwater solid-state lighting,” *Optics Express*, vol. 26, no. 15, pp. 19259-19274, 2018, doi: 10.1364/OE.26.019259.
- [27] T. Zhang, X. Zhang, B. Ding, J. Shen, Y. Hu, and H. Gu, “Homo-epitaxial secondary growth of ZnO nanowire arrays for a UV-free warm white light-emitting diode application,” *Applied Optics*, vol. 59, no. 8, pp. 2498-2504, 2020, doi: 10.1364/AO.385656.
- [28] M. A. Juratli *et al.*, “Noninvasive label-free detection of circulating white and red blood clots in deep vessels with a focused photoacoustic probe,” *Biomedical Optics Express*, vol. 9, no. 11, pp. 5667-5677, 2018, doi: 10.1364/BOE.9.005667.
- [29] S. K. Abeysekera, V. Kalavally, M. Ooi, and Y. C. Kuang, “Impact of circadian tuning on the illuminance and color uniformity of a multichannel luminaire with spatially optimized LED placement,” *Optics Express*, vol. 28, no. 1, pp. 130-145, 2020, doi: 10.1364/OE.381115.
- [30] O. H. Kwon, J. S. Kim, J. W. Jang, and Y. S. Cho, “Simple prismatic patterning approach for nearly room-temperature processed planar remote phosphor layers for enhanced white luminescence efficiency,” *Optical Materials Express*, vol. 8, no. 10, pp. 3230-3237, 2018, doi: 10.1364/OME.8.003230.

## BIOGRAPHIES OF AUTHORS



**Ha Thanh Tung**    received the PhD degree in physics from University of Science, Vietnam National University Ho Chi Minh City, Vietnam, he is working as a lecturer at the Faculty of Basic Sciences, Vinh Long University of Technology Education, Vietnam. His research interests focus on developing the patterned substrate with micro- and nano-scale to apply for physical and chemical devices such as solar cells, OLED, photoanode. He can be contacted at email: tunght@vlute.edu.vn.



**Huu Phuc Dang**    received a Physics Ph.D degree from the University of Science, Ho Chi Minh City, in 2018. Currently, he is a lecturer at the Faculty of Fundamental Science, Industrial University of Ho Chi Minh City, Ho Chi Minh City, Vietnam. His research interests include simulation LEDs material, renewable energy. He can be contacted at email: danghuophuc@iuh.edu.vn.